Dyes and Pigments 232 (2025) 112461

Contents lists available at ScienceDirect

Dyes and Pigments

journal homepage: www.elsevier.com/locate/dyepig

Tetra dansylamides substituted cyclen and cyclam macrocycles as fluorescent sensing probes for metal ions and temperature-responsive materials in dopped polymers

Inês Pereira-Gomes [a,1], Frederico Duarte [a,1], Georgi M. Dobrikov [b,**], Ivaylo Slavchev [b], Atanas Kurutos [b,c], Jose Luis Capelo-Martinez [a,d], Hugo M. Santos [a,d], Carlos Lodeiro [a,d,*]

[a] BIOSCOPE Research Group, LAQV-REQUIMTE, Chemistry Department, NOVA School of Science and Technology, FCT NOVA, Universidade NOVA de Lisboa, 2829-516, Caparica, Portugal
[b] Institute of Organic Chemistry with Centre of Phytochemistry, Bulgarian Academy of Sciences, Acad. G. Bonchev str., bl. 9, 1113, Sofia, Bulgaria
[c] University of Chemical Technology and Metallurgy, 8 St. Kliment Ohridski blvd, 1756, Sofia, Bulgaria
[d] PROTEOMASS Scientific Society, 2825-466, Costa de Caparica, Portugal

ARTICLE INFO

Keywords:
Polymers
Dansyl derivatives
Metal ions
Sensors
Solvatochromism
Temperature

ABSTRACT

Two novel tetra-dansyl derivatives incorporating cyclen (1,4,7,10-tetraazacyclododecane) and cyclam (1,4,8,11-tetraazacyclotetradecane) macrocycles have been synthesized, thoroughly characterized, and their photophysical properties examined, both in solution and in the solid state. These compounds exhibit fluorescence emission with quantum yields up to 40 %, varying significantly with different solvents. They also display positive solvato-fluorochromic behavior, with emissions ranging from green to yellow colours. Kamlet-Taft studies were conducted to better understand solute-solvent interactions. Furthermore, aggregation-induced emission was observed in solutions with high water content, confirmed via dynamic light scattering. Given the intrinsic properties of these compounds, their potential for environmental remediation was explored through metal ion sensing studies. Compounds **L1** and **L2** demonstrated high sensitivity to Cu^{2+} and Hg^{2+} ions, significantly modulating their emission, with **L2** capable of detecting and quantifying Hg^{2+} concentrations as low as 2–3 μM. Additionally, the solid-state emission of these compounds encouraged an investigation into their potential as temperature sensors. Several doped polymer thin films were fabricated, establishing a linear relationship with temperature beyond their melting point. These findings suggest that these tetra-chromophoric compounds hold promise as molecular thermometers.

1. Introduction

Probes and sensors employing fluorescent dyes are highly beneficial due to their exceptional optical features. Among this extensive group, dansyl derivatives have consistently been used throughout the decades amidst their consistent photophysical properties, namely large Stokes shift, high fluorescence quantum yields and the well-known strong dependence of the emission properties on the surrounding environment [1–5]. The detection of heavy metals and transition metal ions is extensively documented in the literature, given the wide range of applications to which dansyl derivatives have been put to use, especially for Cu^{2+} [1,2,4,6–10], Zn^{2+} [11,12], Ag^{2+} [13], Cd^{2+} [14], Hg^{2+} [1,4,15–18] and Pb^{2+} [19].

Given the current efforts to develop new dyes, aza-crown compounds, namely cyclen (1,4,7,10-Tetraazacyclododecane) and cyclam (1,4,8,11-Tetraazacyclotetradecane) were employed as good candidates to their versatility and wide range of applications including in the fields of medicine [20,21], magnetic resonance imaging [22–24], catalysis [25–27] and pollutant degradation [28]. Within this context, azamacrocyclic tetramines can readily be functionalized and demonstrate robust binding to a diverse array of cations [29]. An example of this was demonstrated by Hava Ozay et al. where p(2-hydroxyethyl

* Corresponding author. BIOSCOPE Research Group, LAQV-REQUIMTE, Chemistry Department, NOVA School of Science and Technology, FCT NOVA, Universidade NOVA de Lisboa, 2829-516, Caparica, Portugal.
** Corresponding author.
E-mail addresses: Georgi.Dobrikov@orgchm.bas.bg (G.M. Dobrikov), cle@fct.unl.pt (C. Lodeiro).
[1] These authors have contributed equally to the work.

https://doi.org/10.1016/j.dyepig.2024.112461
Received 25 July 2024; Received in revised form 11 September 2024; Accepted 13 September 2024
Available online 16 September 2024

methacrylate-co-tetraacrylic cyclen) (p(HEMA-co-TACYC)) hydrogels were synthesized with the intention to transfer the copper ion binding ability of cyclen into the hydrogel structure. The designed hydrogels showed selective colorimetric sensor behaviour towards Cu^{2+} in all aqueous media and when submitted to metal ion mixtures [30].

Functionalization of these macrocycles with fluorophores is supported by the literature, namely with anthracene, naphthalimide, rhodamine and BODIPY [29,31,32]. Xiao Fang et al. have synthesized a BODIPY-based fluorescent probe with a cyclen moiety that improved water solubility, followed by Cu^{2+} binding. The selective turn-on fluorescent behaviour for H_2S was elucidated with a LOD of 1.1 nM. Additionally, the complex was effectively utilized for imaging exogenous H_2S generated from Na_2S and GYY4137 in H9c2 and U87 cells [31].

Based on an extensive literature search, the dansylation of aza-crown compounds is in its early stages with very early reports focused on mono dansylated cyclen [33,34]. More recently, this compound was used for the formation of metal complexes in various matrices [35–38]. The presence of metal ions binding to the basic nitrogen atoms of this derivative is crucial for the creation of a stable complex. Rivas et al. demonstrated that coordination of metal ions with other heteroatoms outside the aza-crown ring is also feasible [39]. Due to the negligible cytotoxicity, good penetration and photostability, Yang et al. have been successful in using this compound for specific lysosome labeling in various cell lines [40]. To the best of our knowledge, only a few mentions of dansyl derivatives of cyclam are reported in the art [41–45]. In this study, we successfully synthesized symmetric tetra dansyl derived compounds of cyclam and cyclen for the first time. These newly developed fluorophores were then fully characterized according to their photophysical properties. The Kamlet-Taft equation was used to explain the solvatochromism behaviour of functionalizing the aza-crown with four dansyl units. The tuning of the emission using water as co-solvent led to an aggregation induced emission in high water fraction and was confirmed by dynamic light scattering. The above-mentioned ligands were designed in order to demonstrate good complexation ability toward heavy metals and so efforts to elucidate their ability to sense pollutant metal ions was put forth. Finally, incorporation into polymer thin films KURARITY (L44285) and IROGRAN (A 92 P 4637) towards the development of temperature-smart materials was carried out.

2. Experimental section

2.1. Materials

Spectroscopy grade solvents, such as acetonitrile (CH_3CN), chloroform ($CHCl_3$), dimethylsulfoxide (DMSO), ethanol (EtOH), and tetrahydrofuran (THF), were used for spectrophotometric and spectrofluorimetric measurements. All solvents used for the synthesis and purification of the target compounds (dichloromethane (DCM) and methyl-*tert*-butyl ether (MTBE)) were of analytical grade (p.a.) and dried over molecular sieve (3 Å). The starting fine chemicals (cyclam (1,4,8,11-Tetraazacyclotetradecane), cyclen (1,4,7,10-Tetraazacyclododecane), diisopropylethylamine (DIPEA) and dansyl chloride) used for the synthesis of the target fluorophores were purchased from Sigma Aldrich, Tokyo Chemical Industry Co. Ltd., and BLDPharm. Silica gel (high-purity grade, pore size 60 Å, 230–400 mesh particle size, 40–63 μm particle size, for flash chromatography) employed for the column chromatography was purchased from Sigma Aldrich. Trifluoromethanesulfonate salts of $Co(OTf)_2$, $Ni(OTf)_2$, $Cu(OTf)_2$, $Zn(OTf)_2$, $Ag(OTf)$, $Cd(OTf)_2$, were provided from Solchemar, while $Hg(OTf)_2$ and $Ca(BF_4)_2H_2O$ were purchased from Sigma Aldrich. KURARITY™ LA4285 Kurashiki, Okayama, Japan; the thermoplastic polyurethane TPU-A92 was offered by Huntsman (Germany). The perfluoroalkoxy (PFA) supports for the fabrication of polymer films were purchased to Bohlender, Gmbh, Germany. Mili-Q ultrapure water was used in all experiments.

2.2. Instrumentation

The chemical identities of the compounds under investigation were confirmed through the utilization of various analytical techniques, including ^{1}H NMR, ^{13}C NMR, DEPT-135, 2-D COSY, 2D-HSQC, and 2-D HMBC NMR spectroscopic techniques. The ^{1}H NMR and ^{13}C NMR spectra were acquired on a Bruker Avance II+600 spectrometer (Institute of Organic Chemistry with Centre of Phytochemistry - Bulgarian Academy of Sciences/NMR Centre) using 5 mm tubes. The measurements were performed in $CDCl_3$ at 293K, with operating frequencies of 600.13 MHz and 150.92 MHz for the ^{1}H- and ^{13}C- nuclei, respectively. The ^{1}H- and ^{13}C- nuclear magnetic resonance (NMR) spectra were standardized using the reference signal of $CDCl_3$ with a chemical shift value (δ) of 7.26 ppm for the ^{1}H NMR and 77.16 ppm for the ^{13}C NMR, respectively. The precision of chemical changes is determined at a level of 0.01 ppm. The coupling constants (*J*) are displayed with a precision of 0.1 and denoted in units of hertz (Hz). The spin multiplicity observed in the 1H- nuclear magnetic resonance (NMR) spectroscopy was represented using the following abbreviations: s for singlet, d for doublet, t for triplet, q for quartet, dd for doublet of doublets, dt for doublet of triplets, td for triplet of doublets, and m for multiplet. MestreNova v. 14.1.1 (Mestrelab Research S.L.) was used for processing the spectra. High-Resolution Mass Spectrometry analyses have been performed in the Laboratory for Biological Mass Spectrometry–Isabel Moura (PROTEOMASS Scientific Society Facility), using UHR ESI-Qq-TOF IMPACT HD (Bruker-Daltonics, Bremen, Germany). Samples of the corresponding compounds were prepared by dissolution in 50 % (v/v) Acetonitrile containing 0.1 % (v/v) aqueous formic acid to obtain a working solution of 0.1 μg/mL. Mass spectrometry analysis was carried out by the direct infusion of the compound solutions into the ESI source. MS data were acquired in positive polarity over the mass range of 80–1300 m/z. (Capillary voltage: 4500 V, End plate offset: −500 V, Charging voltage: 2000 V, Corona: 4000 nA, Nebulizer gas: 0.4 Bar, Dry Heater: 180 °C, Dry gas: 4.0 L/min).

UV–Vis absorption spectra were recorded on a JASCO V-650 spectrophotometer and the fluorescence emission spectrum on a HORIBA Scientific FLUOROMAX-4 spectrofluorometer from BIOSCOPE-PROTEOMASS facilities. Otherwise stated, all photophysical experiments were carried out at 293 K using a quartz cell with 10 mm of optical path.

2.3. Synthetic procedures

2.3.1. General procedure (GP) for the synthesis of L1 and L2

Cyclic tetramine (1.0 eq. of **2** or **3**) and dry DIPEA (8.0 eq.) were dissolved in 50 mL dry DCM, and the formed clear solution was cooled down to 5 °C with ice-water. Dansyl chloride (4.5 eq.) was added in one portion and stirring was maintained for 30 min at this temperature. Subsequently, the reaction mixture was stirred for 4 days at r.t. The reaction outcome was monitored by TLC (mobile phase - DCM:MTBE = 100:1 v/v). Workup: the reaction mixture was diluted with DCM and washed consequently with aq. citric acid (x1), aq. K_2CO_3 (x1) and distilled water (x1). The organic phase was dried over anhydr. Na_2SO_4 and the solvent was evaporated to dryness. The crude product was purified by silica gel column chromatography affording compounds **L1** or **L2**, respectively.

2.3.2. Data for 5,5′,5″,5‴-(1,4,7,10-tetraazacyclododecane-1,4,7,10-tetrasulfonyl)tetrakis(N,N-dimethylnaphthalen-1-amine) (L1)

This compound was prepared according to the general synthetic procedure described above using cyclen (**2**) (1.00 mmol, 0.172 g, 1 eq.), DIPEA (8.00 mmol, 1.39 mL, 1.39 mL) and dansyl chloride (4.50 mmol, 1.214 g, 4.5 eq.) (**1**). Column chromatography: stationary phase - 75 g silica gel; Mobile phase - DCM:MTBE = 75:1v/v. The target product **L1** was obtained in 0.984 g (89 %) as a light-yellow powder. m.p. 178–179 °C. ^{1}H NMR (600 MHz, $CDCl_3$) δ 8.57 (d, J = 8.5 Hz, 4H), 8.49

(d, $J = 8.7$ Hz, 4H), 8.01 (dd, $J = 7.4$, 1.2 Hz, 4H), 7.53 (td, $J = 9.0$, 7.5 Hz, 8H), 7.18 (d, $J = 7.1$ Hz, 1H), 3.67 (s, 16H), 2.89 (s, 24H). ^{13}C NMR (151 MHz, $CDCl_3$) δ 151.83, 133.19, 130.79, 130.74, 130.44, 129.63, 128.57, 123.35, 119.82, 115.50, 51.34, 45.56, 0.14. ESI-MS: $[M+H]^+$ for $C_{56}H_{64}N_8O_8S_4$ = 1105.3758 m/z (−4 ppm), calculated $[M+H]^+$ for $C_{56}H_{64}N_8O_8S_4$ = 1105.3803 m/z; $[M+2H]^+$ for $C_{56}H_{64}N_8O_8S_4$ = 533.1937 m/z (−0.1 ppm), calculated $[M+2H]^+$ for $C_{56}H_{64}N_8O_8S_4$ = 533.1938 m/z. EA Found C: 60,21; H: 5.95; N: 9.22 and S: 10.95 %. $C_{56}H_{64}N_8O_8S_4$ requires C: 60.85; H: 5.84; N: 10.14 and S: 11.60 %.

2.3.3. Data for 5,5′,5″,5‴-(1,4,8,11-tetraazacyclotetradecane-1,4,8,11-tetrasulfonyl)tetrakis(N,N-dimethylnaphthalen-1-amine) (L2)

L2 compound was prepared according to the general synthetic procedure described above, employing cyclam (1.00 mmol, 0.200 g, 1 eq.) (**3**), DIPEA (8.00 mmol, 1.39 mL, 1.39 ml) and dansyl chloride (4.50 mmol, 1.214 g, 4.5 eq.) (**1**). Column chromatography: stationary phase - 75 g silica gel; Mobile phase - DCM:MTBE = 25:1 v/v. The target product **L2** was obtained in 1.025 g (90 %) as a light-yellow powder. m.p. 227–228 °C. ^{1}H NMR (600 MHz, $CDCl_3$) δ 8.55 (d, $J = 8.5$ Hz, 4H), 8.33 (d, $J = 8.7$ Hz, 4H), 8.04 (dd, $J = 7.3$, 1.2 Hz, 4H), 7.52 (ddd, $J = 8.5$, 7.5, 1.2 Hz, 8H), 7.17 (d, $J = 7.3$ Hz, 4H), 3.37 (s, 8H), 3.31 (t, $J = 7.0$ Hz, 8H), 2.88 (s, 24H), 1.95 (p, $J = 7.1$ Hz, 4H). ^{13}C NMR (151 MHz, $CDCl_3$) δ 151.89, 133.62, 130.75, 130.33, 130.28, 129.91, 128.50, 123.35, 119.55, 115.48, 48.14, 47.21, 45.55, 27.65, 0.13. ESI-MS: $[M+H]^+$ for $C_{58}H_{68}N_8O_8S_4$ = 1133.4077 m/z (−3.4 ppm), calculated $[M+H]^+$ for $C_{58}H_{68}N_8O_8S_4$ = 1133.4116 m/z; $[M+2H]^+$ for $C_{58}H_{68}N_8O_8S_4$ = 567.2103 m/z (1.6 ppm), calculated $[M+2H]^+$ for $C_{58}H_{68}N_8O_8S_4$ = 567.2094 m/z. EA Found C: 61,13; H: 6.24; N: 9.67 and S: 11.30. $C_{58}H_{68}N_8O_8S_4$ requires C: 61.46; H: 6.05; N: 9.89 and S: 11.32 %.

2.4. Spectrophotometric and spectrofluorimetric measurements

2.4.1. Photophysical characterization and titrations

Photophysical measurements began with the preparation of stock solutions of compounds **L1** and **L2** (*ca.* 10^{-3} M) in various solvents (CH_3CN, DMSO, $CHCl_3$, and THF), by dissolving each ligand in a 10 mL volumetric flask and diluting with the corresponding solvent. The working solutions in the range of $10^{-5} - 10^{-6}$ M were then prepared by dilution of the stock solutions.

Titrations of **L1** and **L2** were performed by successive additions of microliter aliquots of standard solutions of Ca^{2+}, Co^{2+}, Ni^{2+}, Cu^{2+}, Zn^{2+}, Ag^+, Cd^{2+}, Hg^{2+} ions prepared in acetonitrile. A correction for the absorbed light was performed when necessary. The temperature dependent emission spectra were recorded by encapsulating the material between quartz plates, and over a hotplate with temperature control for measurements at variable temperature. Additionally, mixtures containing different water fractions (f_w), ($f_w = 0$ %, 17 %, 33 %, 55 %, 67 % and 83 %) with a final concentration of 10 μM were prepared and characterized by absorption and emission spectroscopy. Luminescence spectra of the compounds in the solid state and of doped polymer thin films were recorded using a fiber-optics device connected to the spectrofluorometer while exciting the samples at appropriated wavelength.

2.4.2. Fluorescence quantum yield and lifetime

The evaluation of the relative photoluminescence quantum yields was performed by preparing a solution of dansylamide in DMSO (ϕ_F = 0.47) as reference standard for quantifying the relative QY of **L1** and **L2** in all studied solvents [46]. Lifetime measurements were recorded on a Tempro Fluorescence Lifetime System with a Horiba Jobin-Yvon NanoLed pulsed diode controller. All measurements were carried out at 293 K.

2.5. Determination of the detection and quantification limits (LOD and LOQ)

Determination of the detection limit (LOD) and quantification limit (LOQ) began by collecting ten independent measurements of a solution containing the selected probe and no addition of any metal ion (y_{blank}). Final determination of the LOD and LOQ values followed the subsequent formulas [47,48].

LOD = $y_{dl} = y_{blank} + 3$std, where y_{dl} = signal detection limit and std = standard deviation.

LOQ = $y_{dl} = y_{blank} + 10$std, where y_{dl} = signal detection limit and std = standard deviation.

The final step involved the determination of the minimal detectable and quantified concentration of metal ion by titration with the ligands.

2.6. Preparation of polymer dye-doped thin films

- **KURARITY** L44285 **film**

Production began by weighting 100 mg of polymer in a vial and was dissolved in 5 mL of chloroform whereas 1 mg of the compound (**L1** or **L2**) was weighted in a separate vial and dissolved in 1 mL of chloroform. Then, the polymer solution was stirred aided by heating at 70 °C and when the polymer was completely dissolved, the compound solution was added, and they were mixed.

- **IROGRAN A 92 P 4637**

TPU's solution was prepared by weighting 100 mg of this polymeric material in a vial and in another vial was weighed 1 mg of the compound. The amount of TPU weighted was dissolved in 10 mL of THF over stirring at room temperature until it was totally dissolved. The dye solution was prepared in THF for **L1**-2 and then added to the polymer solution.

The resulting solution from the mixture of the compound solution and the polymer solution was poured into a perfluoro alkoxy alkane, PFA, support with 5 cm of diameter and left it to slow evaporation at room temperature during *ca.* 24h.

3. Results and discussion

3.1. Synthesis

The synthesis of both compounds **L1** and **L2** was accomplished under classical conditions for the preparation of sulfonamides from amines and sulphochlorides (Scheme 1). Both cyclen (**2**) and cyclam (**3**) were dissolved in dry DCM and reacted with an excess of dansyl chloride (**1**) in the presence of dry DIPEA. Analytical samples of **L1** and **L2** were obtained after column chromatography on silica gel and were fully characterized by 1D and 2D-NMR spectroscopic techniques, HRMS and melting point temperatures.

3.2. Photophysical characterization

The tetradansylated derived compounds of cyclen and cyclam exhibit photoluminescent properties both in solution and in the solid state. Fig. 2 shows the molecular representation side by side with photophysical data of compound **L1** and **L2** in chloroform recorded at 293 K as a representative example (Figs. S5–S6) while the data in all solvents are summarized in Table 2.

Considering the UV–Vis spectra, **L1** and **L2**, show a maximum at *ca.* 344 nm which is assigned to the π - π* transition of dansyl chromophore contributing to the absence of any colour visible to the naked eye. Upon excitation at the appropriate wavelength, the samples emit a greenish light with a maximum centered around 502 nm and 499 nm, characteristic for the dansyl moiety due to the intramolecular charge-transfer

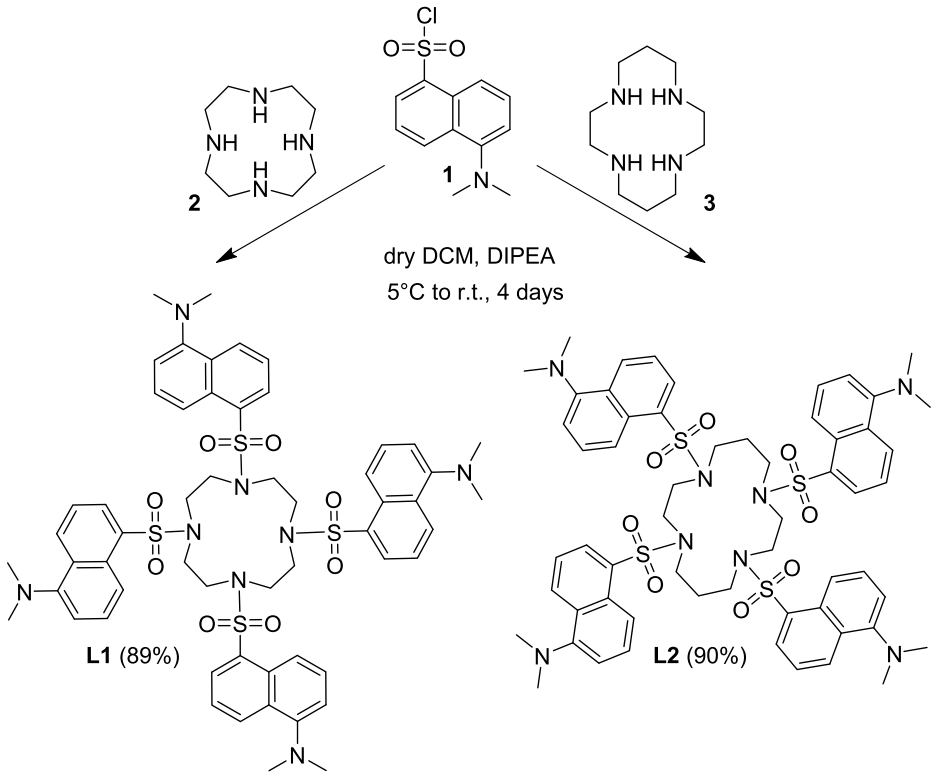

Scheme 1. Synthetic approach to the preparation of the target compounds **L1** and **L2**.

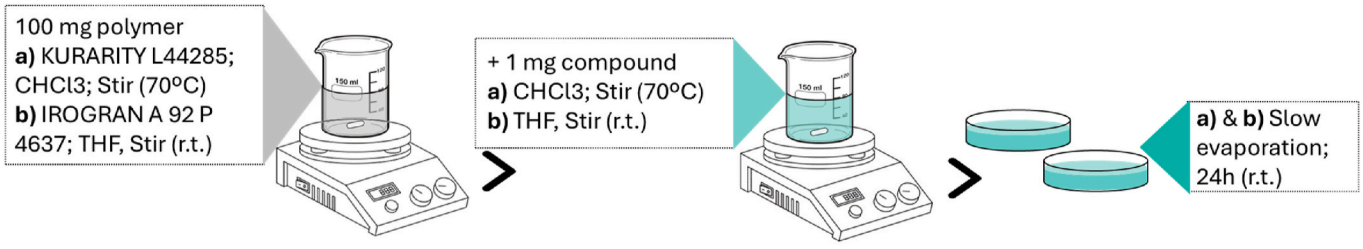

Fig. 1. The method of synthesis of a) KURARITY L44285 and b) IROGRAN 4 92 P 4637 films.

(ICT) band between the N,N′-dimethylamine (donor) and the sulfonamide (acceptor) functions, resulting in a Stokes shift of 9149 and 9029 cm^{-1}. On a relatable note, significant disparities can be noted regarding the solid-state emission spectra on both compounds where a wide band centered at 508 nm is recorded for **L1** much similar to the one in chloroform solution, while for **L2**, a clear, blue-shifted emission is evident accompanied by an emission maximum at 487 nm.

The fluorescence quantum yield has been determined using dansyl amide as a standard for both dansyl derivatives. Significantly higher values of 35 % and 41 % have been attained for **L1** and **L2** in chloroform, while for the remaining solvents, values were in the range of 24–34 %. Double digit nanosecond times were observed from time-resolved fluorescence decay curves for all solvents sitting in the range of 12.4–15.2 ns, however, no relevant association can be determined between the characteristics of the solvent and compounds studied.

However, the presence of a solvent environment significantly affects the stabilization of the ligand's excited state due to the alteration of the fluorophore's dipole moment. Based on the information presented in Table 1, the increase in solvent polarity is accompanied by an increase of the energy gap and, consequently, an increase in Stoke's shift, which translate into a bathochromic shift. The shift presented can be related to a positive solvatofluorochromic effect due to the capacity of the environment-sensitive dyes to change their fluorescence maximum wavelength aligned with the solvent polarity, behaviour well noticed in Fig. 2.

Aligned with these observations, efforts have been made to thoroughly characterize the interactions between the solvent and the compound. To achieve this, three solute-dependent parameters (υ_0, a, b and p) have been determined through the multiparametric fitting of the Kamlet-Taft equation (Equation (1)).

$$\upsilon = \upsilon_0 + a\alpha + b\beta + p\pi^* \quad \text{(Equation 1)}$$

Where υ_0 represents the wavenumber value in a reference solvent; parameters a, b and p are obtained through multiple regression analysis that reflect the underlying sensitivity of the probes photophysical behaviour to solvent polarity; α: hydrogen bond donor acidity (HBD); β: hydrogen bond acceptor basicity (HBA); π*: stabilization of a charge or dipole without a specific dielectric interaction (Table 1) [49,50].

Table 3 presents the reference wavenumber value υ_0, the fitted parameters (a, b and p) alongside the slopes and correlation coefficients obtained through the fitting of a linear plot of $\upsilon_{exp.}$ versus υ_{calc}, by applying the Kamler-Taft model. It is perceptible for both compounds extended negative values of a and b parameters, where some relevant differences are present in the predisposition towards hydrogen bond donor sensitivity being **L2** more slightly prone to be influenced by protic

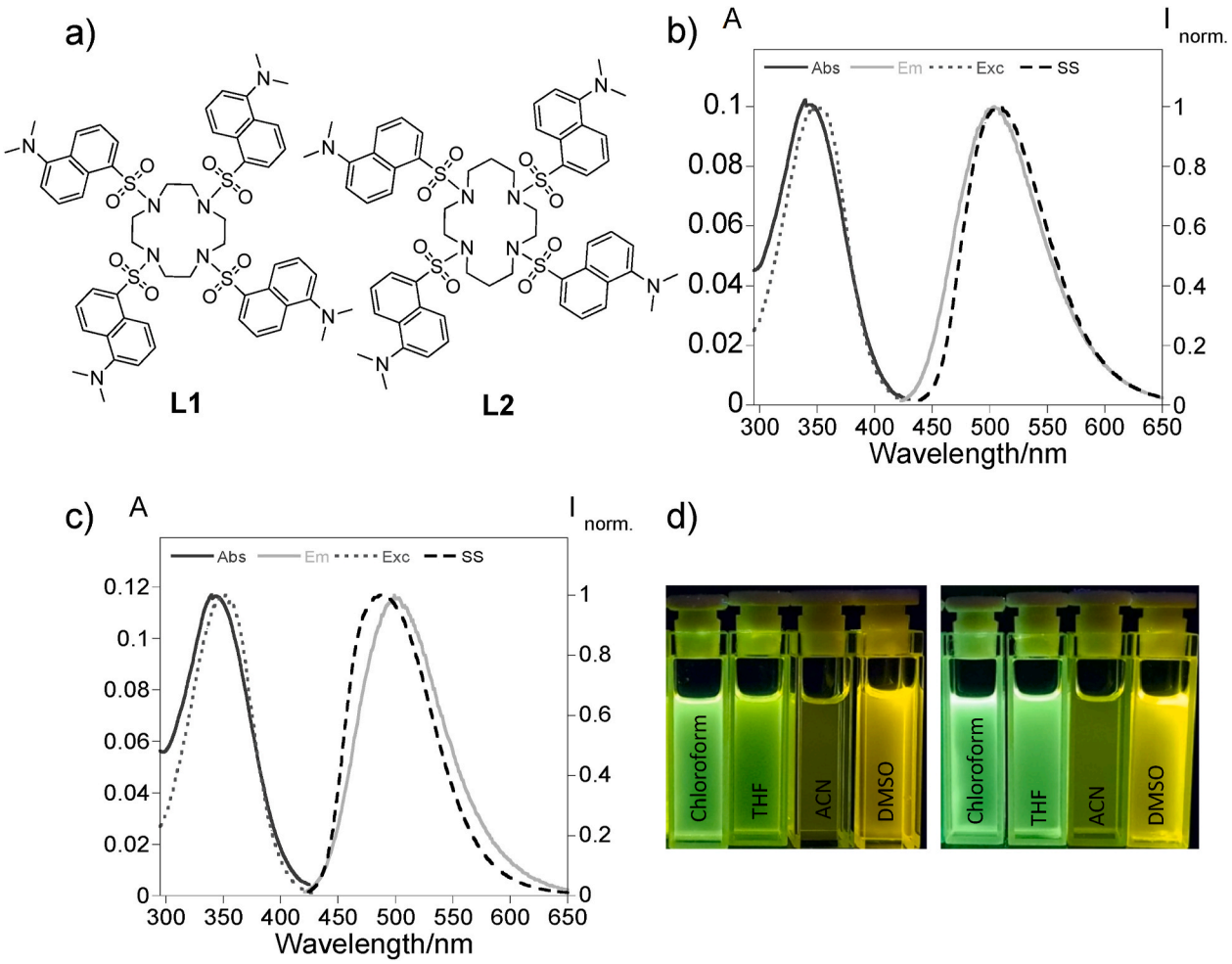

Fig. 2. (a) Molecular structure of tetradansylated cyclen and cyclam derived compounds **L1** and **L2**. Photophysical characterization of derivatives **L1** (b) and **L2** (c) in chloroform ([**L1**] = [**L2**] = 5 μM). Images under UV light for (d) **L1** (left) and **L2** (right) in different solvents.

Table 1
Spectroscopic polarity parameters, physical properties of the different solvents. ε_r: relative permittivity; η: refractive index; α: the solvent's HBD acidity; β: the solvent's HBA basicity; π*: the solvent's dipolarity/polarizability.

Solvent	ε_r	α	β	π*	η
DMSO	47.24	0	0.76	1.00	1.47
ACN	35.94	0.19	0.40	0.66	1.34
THF	7.58	0	0.55	0.58	1.40
$CHCl_3$	4.89	0.20	0.10	0.69	1.44

solvents. Finally, large negative p value observed for **L2** indicate a more instability towards highly polarizable solvents presumably due to the increase in size with less rigidity due to the introduction of two carbons in the macrocycle.

3.3. Exploring the behavior in aqueous media

Solutions with different ratios of water in THF were prepared and measured by absorption and fluorescence emission spectroscopy in

Table 3
Independent fluorescence wavenumber ($\upsilon 0$), solvent polarity (p), HBD (a), HBA (b), slope and coefficient (R^2) of the linear fitting plot $\upsilon_{exp.}$ versus $\upsilon_{calc.}$

	υ_0	a	b	p	Slope	R^2
L1	21795	−6245	−3399	−415	1.00	1
L2	22197	−6548	−3357	−741	1.00	1

Table 2
Absorption maximum wavelength in solution (λ_{abs}), emission maximum wavelength in solution (λ_{em}), molar absorption coefficients (ε), Stokes shift ($\Delta\lambda$), fluorescence quantum yields (ϕ), emission maximum in the solid state (λ_{em}^{Solid}), brightness (ε x ϕ), fluorescence lifetimes (τ) for compounds **L1** and **L2** in various solvents.

Cpd.	Solv.	λ_{abs} [nm]	λ_{em} [nm]	ε (10^4) [cm^{-1} M^{-1}]	Stokes shift [cm^{-1}]	ϕ (%)	λ_{em}^{Solid} [nm]	(ε x ϕ) (10^3) [cm^{-1} M^{-1}]	τ[ns]
L1	DMSO	347	532	2.23	10021	28	508	6.24	13.6
	CH_3CN	344	527	2.38	10094	24		5.71	12.4
	THF	340	508	2.25	9726	30		6.75	15.1
	$CHCl_3$	344	502	2.01	9149	35		7.04	14.8
L2	DMSO	345	529	1.95	10081	34	487	6.63	15.2
	CH_3CN	342	523	2.26	10119	28		6.33	13.4
	THF	340	502	2.09	9491	27		5.64	13.9
	$CHCl_3$	344	499	2.33	9029	41		7.04	15.2

order to evaluate the optical properties of the ligands when exposed to water. Fig. 3 shows that the increase of water content is responsible for a decrease in the emission intensity to 67 % following a bathochromic shift, while at 83 % of water content, an increase on luminescence intensity (ca. 40 %) is evident without a shift when comparing to the initial solution. This increase of emission intensity with water fraction of 83 % translates on a fluorescence quantum yield values increase (φL1 = 49,7 %; φL2 = 50,4 %) than in the absence of water (φL1 = 30 %; φL2 = 27 %), which suggest an aggregation induced emission (AIE) effect, i.e., when in the vast majority of water medium, the ligand molecules tend to aggregate and restrict the intramolecular rotation blocking the non-radiative relaxation [51,52]. While in the presence of 67 % of water, both ligands reveal some solubility issues as shown in Fig. 3, where some precipitate is observed which contributes also to the decrease of the emission signal and clarifies the decrease in the absorption profile.

Initially, when the water content is increased, there is a notable rise in the baseline as seen in the absorption spectra of the solution containing 83 % water. The observed rise in the absorbance measurement can be attributed to a light scattering artifact caused by the presence of aggregates, which adds to the inherent heterogeneity. Through dynamic light scattering, the solutions were measured resulting on different polydispersity index, PDI_{L1} = 0,127; PDI_{L2} = 0.049 with hydrodynamic sizes of 134 ± 3 nm (**L1**) and 98 ± 1 nm (**L2**), and zeta potential of −18 ± 1 mV (**L1**) and −22 ± 2 mV (**L2**). The PDI obtained reflect the presence of monodisperse aggregates for the two compounds, with slightly differences on the size and zeta potential due to the molecular organization in aggregates.

3.4. Metal ions sensing

Considering the possible use of dansyl derivatives for detecting metal ions, we evaluated the capacity of **L1** and **L2** to sense metal ions, including, Ca^{2+}, Co^{2+}, Ni^{2+}, Cu^{2+}, Zn^{2+}, Ag^{+}, Cd^{2+}, Hg^{2+}, which were evaluated in acetonitrile. Fig. 4 illustrates the impact on the emission

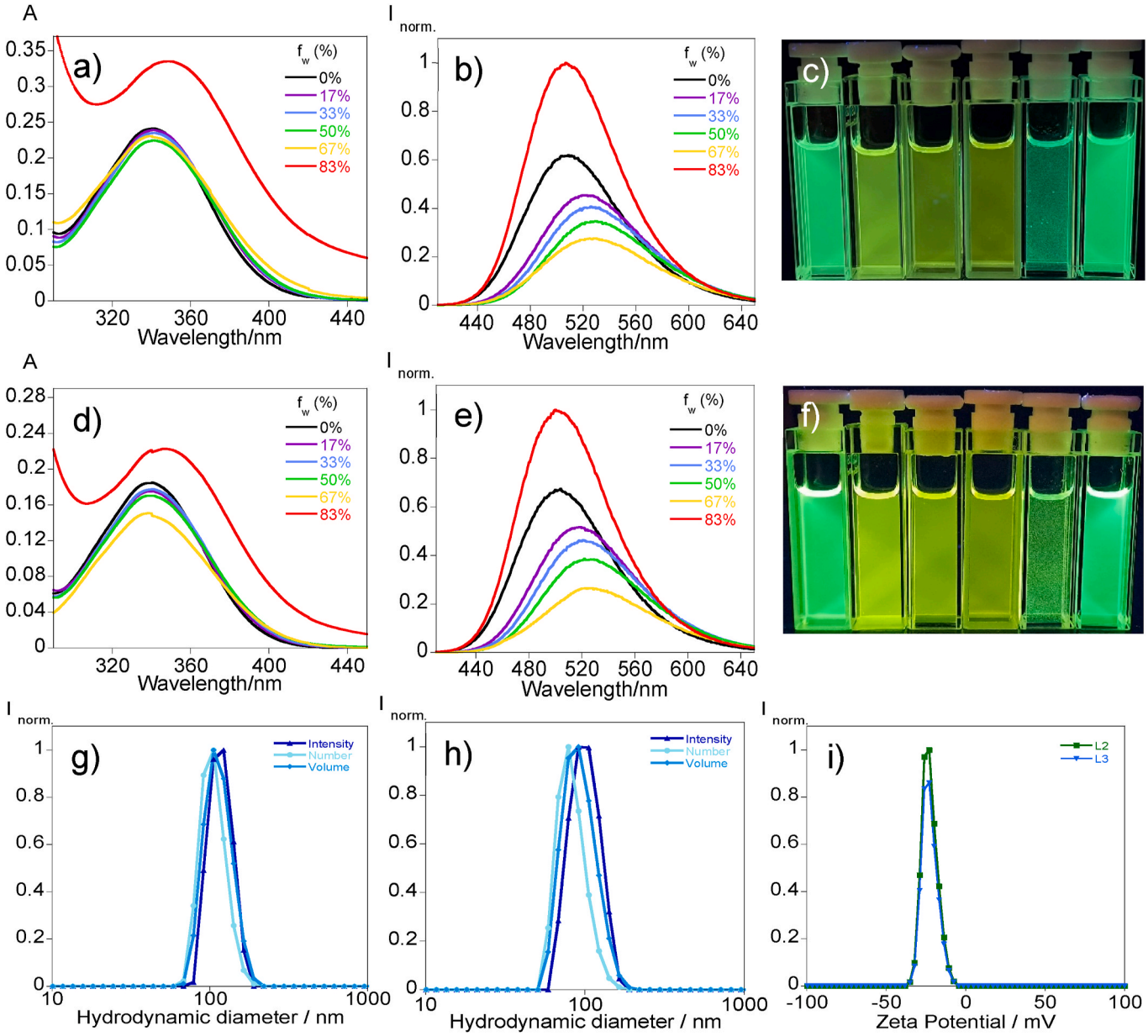

Fig. 3. Absorption (a,d) and emission spectra (b,e) of **L1** (a,b) and **L2** (d,e) in THF with different water fractions f_w (0 %, 17 %, 33 %, 55 %, 67 %, 83 %), [**L1**] = [**L2**] = 10 μM. Images of **L1** (c) and **L2** (f) in THF with different water fractions. Hydrodynamic diameter of **L1** (g) and **L2** (h) aggregates according to number, volume, and intensity distributions and zeta potential (i) of a solution of THF/water with f_w = 83 %.

intensity when 1, 5, and 10 equivalents of the aforementioned metal ions are added. It is evident that the absorption and emission spectra only exhibited significant spectrum alterations in the presence of mercury(II) and copper(II) ions. By adding only 1 equivalent of both metal ions, the emission signal is significantly reduced. Subsequently, adding 5 equivalents completely suppresses the fluorescence intensity. Thus, both compounds exhibit strong selectivity for the specified metal ions.

Thereby, Fig. 5 displays the titrations of **L1** and **L2**, in acetonitrile, upon successive addition of Cu^{2+} (a, c) and Hg^{2+} (b, d) microliter aliquots, respectively, conducted through spectrophoto- and spectrofluorimetric devices.

The progressive addition of Cu^{2+} ions results, generally, in a decrease on both the absorption and the emission spectra. The absorption spectra display a decrease of the main band centered at 345 nm and 342 nm for **L1** and **L2**, respectively. A remarkable decrease in luminescence intensity is also observed without noticing any particular shift of the maxima (530 nm and 522 nm for **L1** and **L2**, respectively). Copper ion is a paramagnetic transition metal with an unfilled d orbital that can induce mechanisms like electron transfer or energy transfer caused quenching, consequently, the quenching in luminescence is observed.

Similarly, as Hg^{2+} solution is gradually added, a decrease is noted on the main absorption band at 344 nm without any shift. Looking to the spectrofluorimetric data, at 525 nm for **L1**, a quenching of the emission's intensity occurs, causing an almost complete suppression upon added 2 equivalents of the metal ion and, consequently, the formation of a plateau. Attending to Fig. 5 (c and d), an analogous behaviour is verified for **L2**. Hg^{2+} ions exhibit diamagnetic properties with a d^{10} configuration and large atomic number, in that case, the formation of heavy atom complexes can lead to non-radiative deactivation explaining the observations.

Therefore, considering that in the presence of Cu^{2+} and Hg^{2+}, both ligands show an absorption and a fluorescence decay, while a chelation enhanced quenching effect (CHEQ) phenomenon is suggested, where **L1** and **L2** coordinate to the metal ion resulting in the corresponding complexes evidenced by Fig. 6 [53–61].

In order to completely assess the sensing ability towards Hg^{2+} and Cu^{2+}, the HypSpec software [62] was used for the calculation of the interaction constants of all complexes. Furthermore, the determination of the detection and quantification limit parameters of both compounds towards both has been fulfilled. The association constants, LOD and LOQ are included in Table 4.

The stability constants were evaluated based on the stoichiometry 1:1 (L:M) by keeping in mind the complex centers evidenced by the ligand structures. The stability constants values for **L1** and **L2** towards both metal ions clarify the high affinity between both species being the highest constant found for **L2** towards Cu^{2+} with a value of $LogK_{ass.} = 5.870 \pm 0.003$. Thus, detectable differences rise while considering the two macrocycles specially for Cu^{2+} sensing in the observed values since the presence of two more carbons provide the flexibility to better accommodate the metal ion.

The lowest detectable and quantifiable amounts were determined for **L2** (2.0 μM and 3.0 μM), having the potential to be useful in applications such as environmental monitoring, where the presence of Hg^{2+} needs to be detected and quantified at low concentrations.

3.5. *Designing Temperature-Responsive materials using dansyl derivative emission*

Since **L1** and **L2** have shown solid-state emission and exhibit solvatofluorochromism due to the varying properties of different solvents,

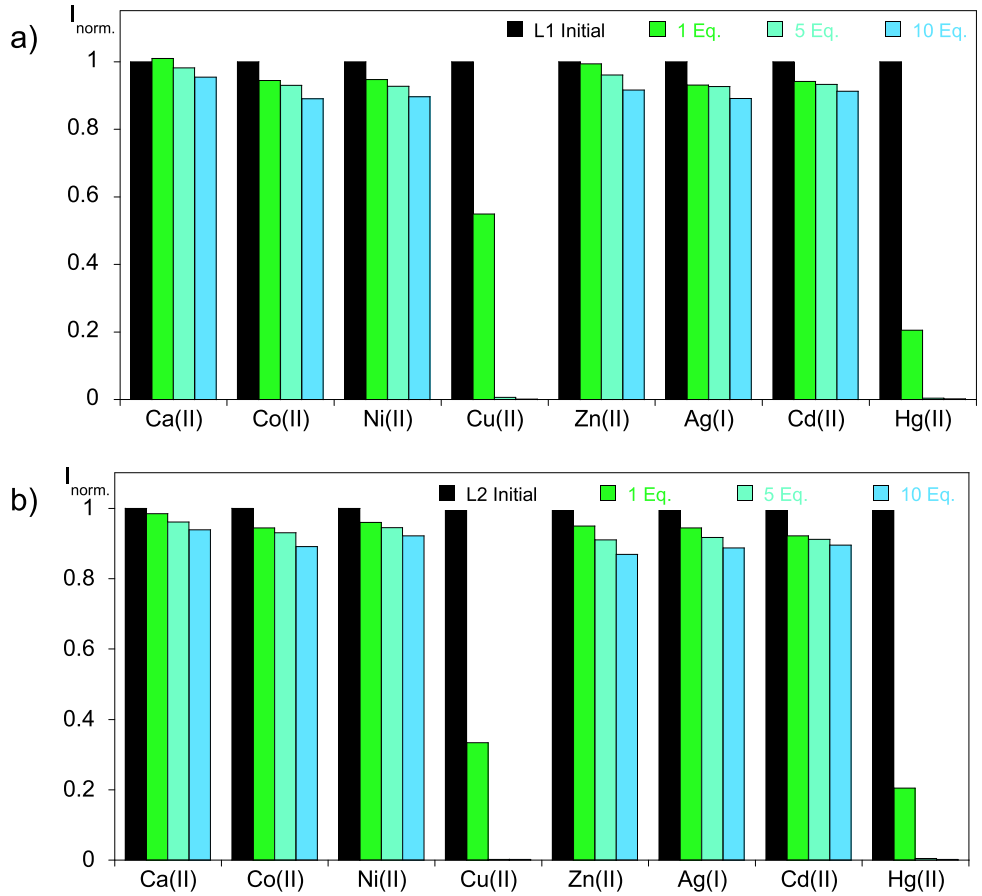

Fig. 4. Normalized emission intensity of **L1** (a) and **L2** (b) upon addition of 1, 5, and 10 equivalents of Ca^{2+}, Co^{2+}, Ni^{2+}, Cu^{2+}, Zn^{2+}, Ag^{+}, Cd^{2+}, and Hg^{2+} metal ions in acetonitrile. ([**L1**] = [**L2**] = 5 μM, T = 298K).

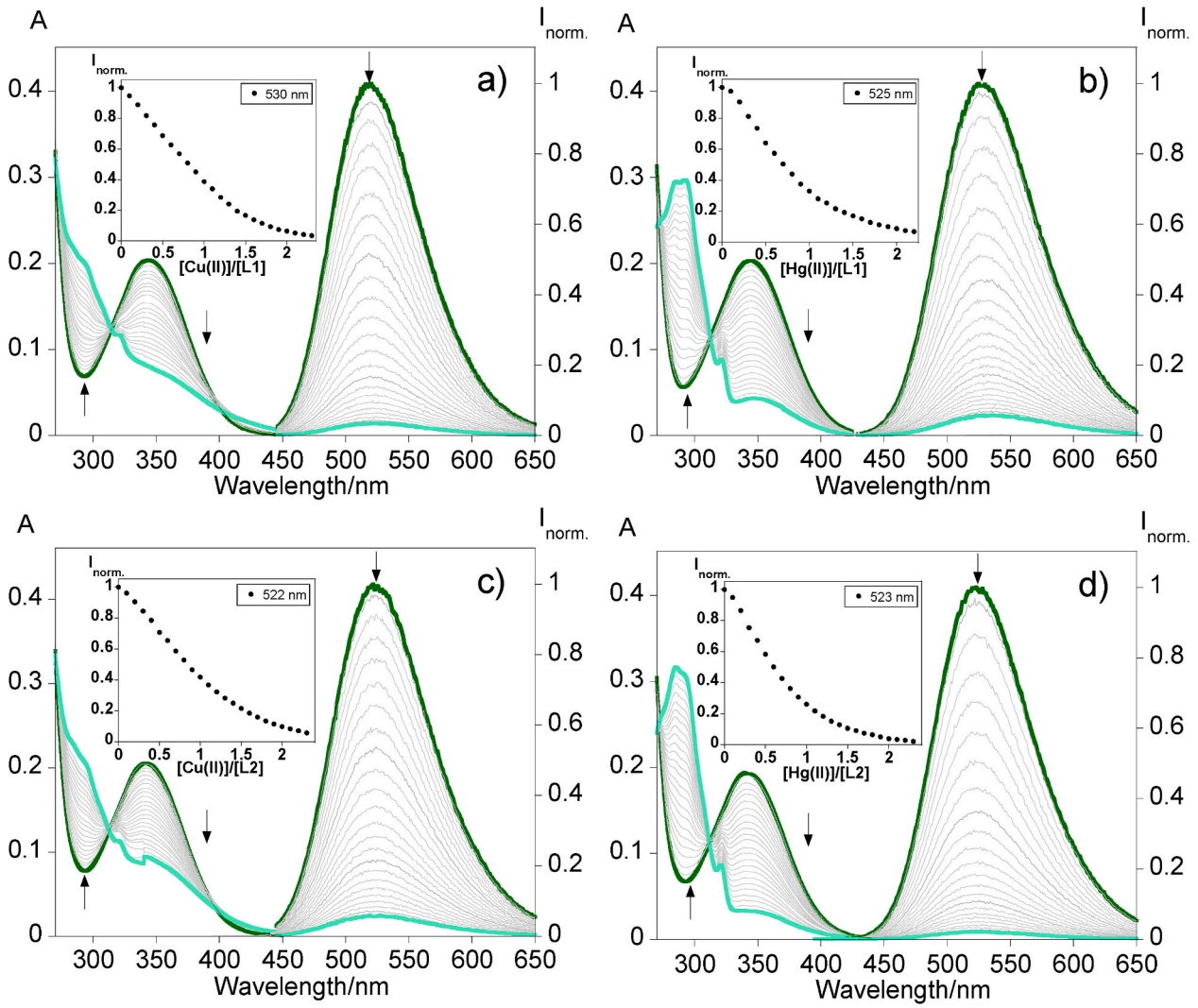

Fig. 5. Spectrophotometric and spectrofluorimetric titrations of compounds **L1** (a, b) and **L2** (c, d) with increased additions of Cu^{2+} (a, c), and Hg^{2+} (b, d) in CH_3CN. The inset represents the emission (a–d) as a function of $[Cu^{2+}]/[\mathbf{L1}]$ at 530 nm (a), of $[Cu^{2+}]/[\mathbf{L2}]$ at 525 nm (c), of $[Hg^{2+}]/[\mathbf{L1}]$ at 525 nm (b) and of $[Hg^{2+}]/[\mathbf{L2}]$ at 523 nm (d). [**L1**] = [**L2**] = 5 μM, T = 298 K).

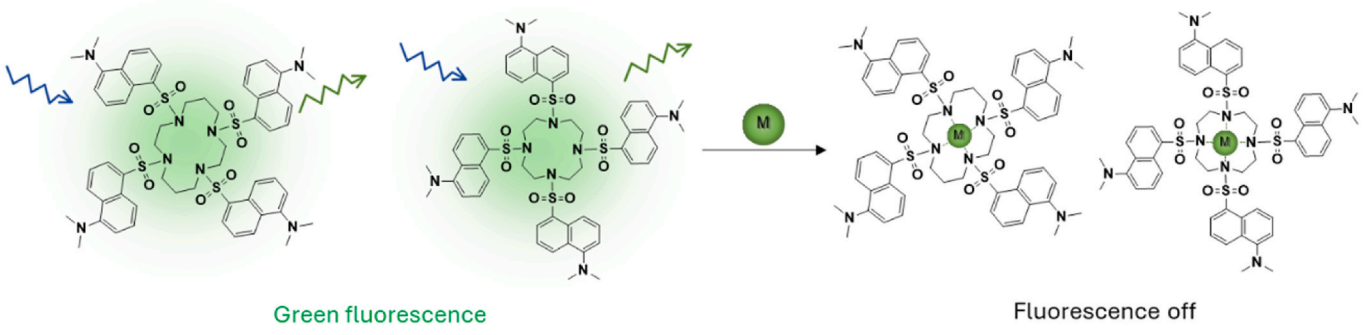

Fig. 6. General representation of the chelation enhanced quenching effect after complexation with Cu^{2+} and Hg^{2+} metal ions.

the next step is to modulate the emission of these ligands in solid-supported materials to develop molecular thermometers based on their emission properties. Initially, these compounds have been studied without the use of solid supports. To this end, the emission of each probe was recorded as the temperature increased in the solid state. Fig. 7 presents the emission spectra and the plot of I_{norm} versus temperature for compound both compounds. While heating, both compounds display a quenching in the fluorescence emission, linear at certain ranges, in the case of **L1**, with no visible shift with respect to the maxima band. Between ca. 40 °C–110 °C a linear behaviour is evident, therefore, within this range, this ligand can function as a probe in optical sensing due to its photochemical stability. However, around 120 °C, a sudden decrease in intensity was observed compromising the recovery of luminescence (only *ca.* 20 %, Fig. S7). The decrease in the fluorescence intensity with

Table 4
Association constants using HypSpec software for compounds **L1** and **L2** towards Hg^{2+} and Cu^{2+} ions with included stoichiometry in acetonitrile. Respective values for the detection limit (LOD) and quantification limit (LOQ) amounts (μM) were measured by the emission at 509 and 513 nm for **L1** and **L2**, respectively.

Compounds	Metal (M)	Association constants ($LogK_{ass.}$), L:M	LOD (μM)	LOQ (μM)
L1	Cu^{2+}	5.613 ± 0.002	2.9	3.4
	Hg^{2+}	5.104 ± 0.002	3.5	3.8
L2	Cu^{2+}	5.870 ± 0.003	2.8	4.4
	Hg^{2+}	5.047 ± 0.002	2.0	3.0

increasing temperature is caused by the loss of intermolecular interactions that leads to the melting point observed at 178 °C in the case of **L1**.

In another way, **L2** can maintain a steady emission and there is no observation of a sharp quenching on the fluorescence intensity until 200 °C due to the higher melting point observed for this compound at 227 °C, characteristic that provides the recovery of *ca.* 90 % of the emission (Fig. S7).

Building on previous findings, several doped polymer thin films have been developed to enhance sensing applications. Following the synthesis procedure of Fig. 1, compounds **L1** and **L2** were doped into Kurarity and TPU. Fig. 8 compares the emission spectra of these compounds in their solid state with their emission in the various polymer thin films.

In summary, polymer thin films were effectively created, and their emission characteristics were examined. Fig. 8 clearly shows that the Kurarity of the polymer matrix can adjust the final emission of the film by interacting with the probe, causing a blue shift in the emission to 480 nm for both compounds. On another hand, the Irogran films maintain the emission maximum wavelength observed in the solid state. Similar behaviours have been observed in a previous work demonstrating the modulation of the emission using polymer matrix of dansyl derivatives [1].

Considering the previous results, the polymer-doped films were studied under varying temperatures to determine if the constraints found in the solid state for **L1** and **L2** could be mitigated. Fig. 9 presents the temperature dependent emission spectra of **L1** doped in both Kurarity and Irogran polymer matrixes as a representative example. The emission spectra for polymer-doped films of **L2** can be found in Fig. S8.

An attenuation of the emission is observed in both polymer-doped films as the temperature increases, up to a maximum of 200 °C. Intriguingly, the behavior of **L1** in its solid state, as influenced by its melting point, does not have an impact on the emission profile in Kurarity. In this case, the polymer matrix functions as a medium to maintain emission at higher temperatures by offering adequate conductivity, thereby reducing the thermally activated non-radiative processes displayed by the compounds and prevent the melting. During the temperature variation cycle, it is possible to perceive linearity from 40 °C to 200 °C and a recovering to 80 % of the initial fluorescence is observed after cooling. Regarding the Irogran doped material, it exhibited the

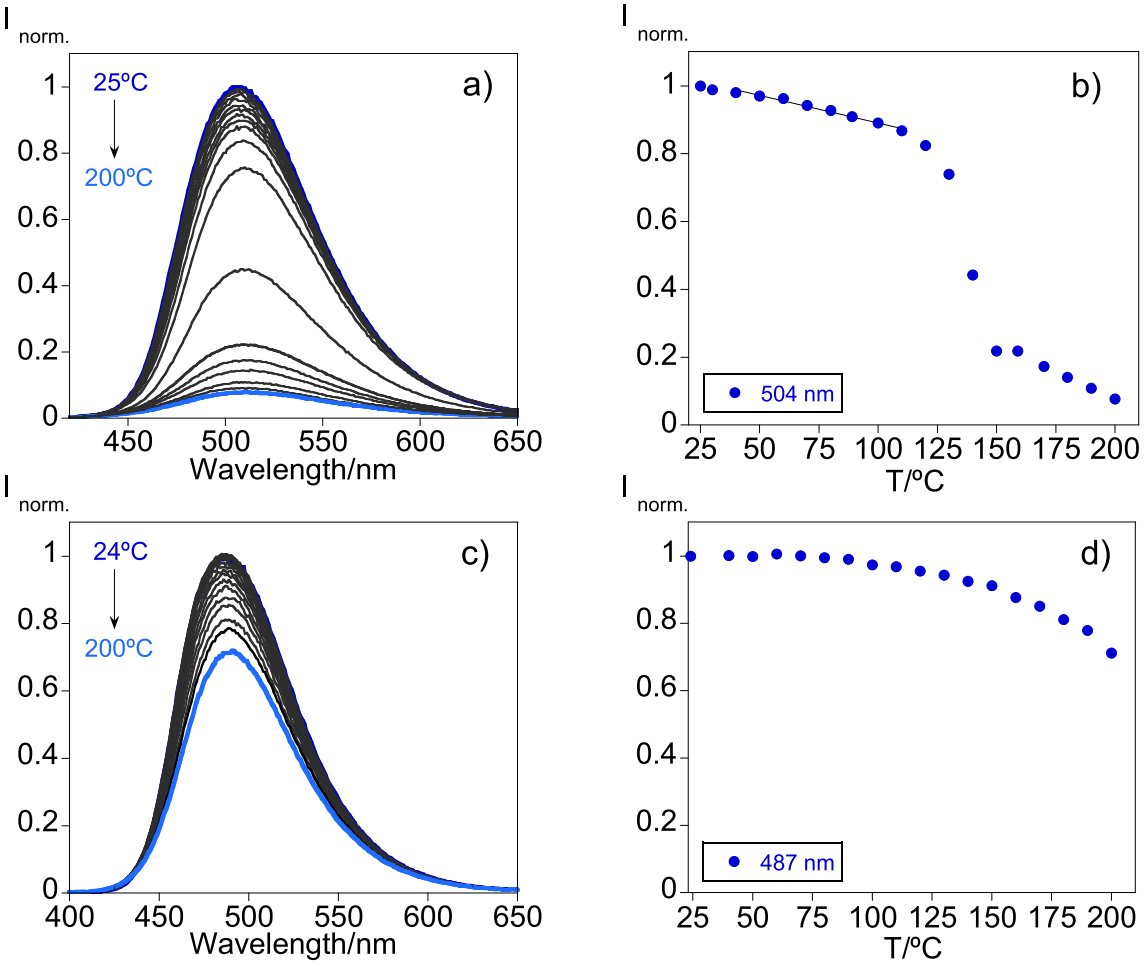

Fig. 7. Temperature-dependent emission spectra of **L1** in the solid state (a) collected through a warming cycle between 25 °C to 200 °C. $I_{norm.}$ vs. T plot recorded in the emission maximum at 504 nm upon heating (b) [40 to 110 °C (Y = 1.0529 - 0.0016231x), yielding R = 0.99139]. Temperature-dependent emission spectra of **L2** (d) collected through a warming cycle between 24 °C to 200 °C. $I_{norm.}$ vs. T plot recorded in the emission maximum at 487 nm upon heating (d).

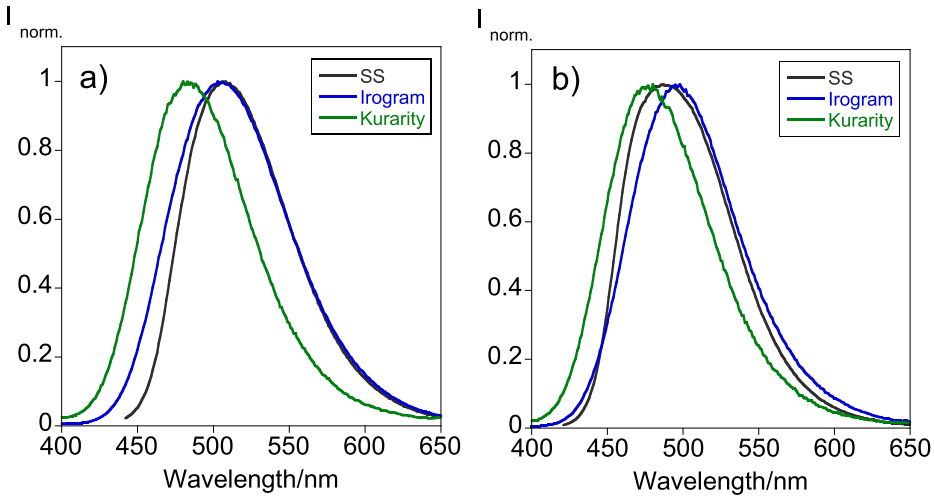

Fig. 8. Comparison between the emission spectra of the different polymer thin films doped with (a) L1 and (b) L2 and the respective emission spectrum in the solid state.

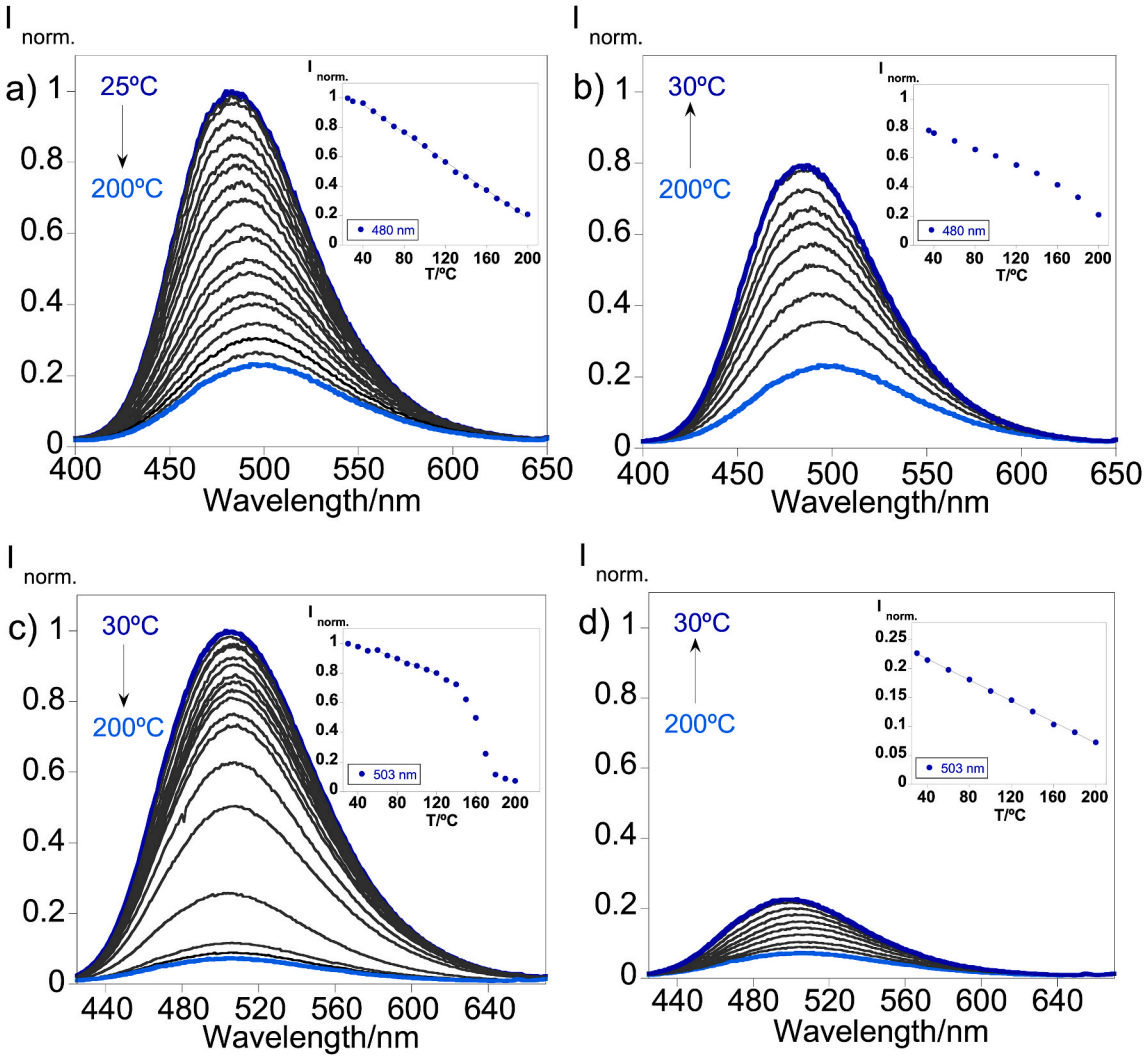

Fig. 9. Temperature-dependent emission spectra of **L1** doped in (a) Kurarity during heating cycle [Inset: $I_{norm.}$ vs. T plot at 480 nm upon heating: 40 to 200 °C (Y = 1.151 - 0.004844x), yielding R = 0.9975]; (b) Kurarity during cooling cycle [Inset: $I_{norm.}$ vs. T plot at 480 nm upon cooling]; (c) Irogran during heating cycle [Inset: $I_{norm.}$ vs. T plot at 503 nm upon heating: 60 to 120 °C (Y = 1.099 - 0.00251x), yielding R = 0.9916]; (d) Irogran during cooling cycle [Inset: $I_{norm.}$ vs. T plot at 503 nm upon cooling: 30 to 200 °C (Y = 0.2527 - 0.0009083x), yielding R = 0.9989].

same behavior as in its solid state, which hindered the restoration of the emission at the end of the cycle.

In the case of **L2** doped materials (Fig. S8) similar ranges of linearity have been found when doped in Kurarity with also almost complete recovery of the emission while for Irogran the fast quenching at 150 °C hampered the emission rise at 25 °C to reach past 25 %. These data show that by attaching the probe to a solid substrate, it can be used as a molecular thermometer without being limited by its physical properties.

4. Conclusions

Two fluorophores, based on tetradansylated cyclen and cyclam, were synthesized and their photoluminescent characteristics were investigated. Efforts were undertaken to study the photophysical features of dansyl compounds in various solvents to fully understand the impact of each solvent's intrinsic properties on the emission of the probes, considering that dansyl compounds commonly display solvatofluorochromism. Implementation of the Kamlet-Taft equation expressed in detail the solute-solvent interactions with a positive solvatofluorochromism behaviour is present for both compounds. Furthermore, the compounds were found to modulate their emission in the presence of water expressing aggregation induced emission at high water content that was confirmed by dynamic light scattering experiments with hydrodynamic sizes of 134 ± 3 nm (**L1**) and 98 ± 1 nm (**L2**). From an environmental remediation perspective, **L1** and **L2** were found to quench their emission in the presence of Hg^{2+} and Cu^{2+} ions. Mononuclear species were proposed with Cu^{2+} and Hg^{2+} and that **L2** has the highest association constant with Cu^{2+} (Log $K_{ass.}$ = 5.87) while the lowest LOD and LOQ was found for Hg^{2+} of 2 μM and 3 μM, respectively. Finally, the probes were characterized in the solid state and incorporated into solid supports to develop molecular thermometers. Polymers such as Kurarity and TPU were doped with the compounds, and their luminescence properties were studied. The polymer matrix Kurarity was discovered to regulate the emission maxima for both compounds. The probes demonstrated excellent linearity throughout the heating cycle, rendering them highly appropriate for utilization as temperature sensors in industrial applications.

Funding

This work received support from PT national funds (FCT/MCTES, *Fundação para a Ciência e Tecnologia* and *Ministério da Ciência, Tecnologia e Ensino Superior)* through the projects UIDB/50006/2020 and UIDP/50006/2020. This work received support from PROTEOMASS Scientific Society through the General Funding Grant 2022–2023, and the projects #PM001/2019 and #PM003/2016. This work is also developed and acknowledged by A.K. as part of contract N♲: BG-RRP-2.004-0002-C01, Laboratory of Organic Functional Materials (Project BiOrgaMCT), Procedure BG-RRP-2.004 „Establishing of a network of research higher education institutions in Bulgaria “, funded by BULGARIAN NATIONAL RECOVERY AND RESILIENCE PLAN“.

CRediT authorship contribution statement

Inês Pereira-Gomes: Writing – review & editing, Validation, Software, Investigation, Formal analysis, Data curation. **Frederico Duarte:** Writing – review & editing, Writing – original draft, Visualization, Validation, Software, Methodology, Investigation, Formal analysis, Data curation. **Georgi M. Dobrikov:** Writing – review & editing, Visualization, Validation, Resources, Investigation, Funding acquisition, Data curation. **Ivaylo Slavchev:** Writing – review & editing, Validation, Investigation. **Atanas Kurutos:** Writing – review & editing, Visualization, Validation, Resources, Methodology, Funding acquisition, Formal analysis, Conceptualization. **Jose Luis Capelo-Martinez:** Writing – review & editing, Writing – original draft, Visualization, Resources, Funding acquisition. **Hugo M. Santos:** Writing – review & editing, Writing – original draft, Visualization, Validation, Resources, Investigation, Formal analysis, Data curation. **Carlos Lodeiro:** Writing – review & editing, Writing – original draft, Validation, Supervision, Resources, Project administration, Funding acquisition, Formal analysis, Conceptualization.

Declaration of competing interest

The authors declare that they have no known competing financial interests or personal relationships that could have appeared to influence the work reported in this paper.

Data availability

Data will be made available on request.

Acknowledgements

This work was supported by the Associate Laboratory for Green Chemistry LAQV which is financed by national funds from *Fundação para a Ciência e Tecnologia and Ministério da Ciência, Tecnologia e Ensino Superior* (FCT/MCTES) through the projects UIDB/50006/2020 and UIDP/50006/2020. PROTEOMASS Scientific Society (Portugal) is acknowledged by the funding provided through the General Funding Grant 2022–2023, and by the funding provided to the Laboratory for Biological Mass Spectrometry Isabel Moura (#PM001/2019 and #PM003/2016). F.D. thanks to FCT/MCTES (Portugal) for his doctoral grant 2021.05161.BD. H. M. S. acknowledges the Associate Laboratory for Green Chemistry LAQV (LA/P/0008/2020) funded by FCT/MCTES for his research contract. The financial support by the Bulgarian National Science Fund (BNSF) under grant – "Novel styryl and polymethine fluorophores as potential theranostic agents "contract N○ КП-06-М59/1 from November 15, 2021 is gratefully acknowledged by A.K. This work is also developed and acknowledged by A.K. as part of contract N♲: BG-RRP-2.004-0002-C01, Laboratory of Organic Functional Materials (Project BiOrgaMCT), Procedure BG-RRP-2.004 „Establishing of a network of research higher education institutions in Bulgaria“, funded by BULGARIAN NATIONAL RECOVERY AND RESILIENCE PLAN“.

G. D. thanks to the European Regional Development Fund within the Operational Programme Science and Education for Smart Growth 2014–2020 under the Project Center of Excellence: National center of mechatronics and clean technologies - BG05M2OP001-1.001-0008 for the financial support.

Appendix A. Supplementary data

Supplementary data to this article can be found online at https://doi.org/10.1016/j.dyepig.2024.112461.

References

[1] Duarte F, Dobrikov G, Kurutos A, Capelo-Martinez JL, Santos HM, Oliveira E, Lodeiro C. Development of fluorochromic polymer doped materials as platforms for temperature sensing using three dansyl derivatives bearing a sulfur bridge. J Photochem Photobiol Chem 2023;445:115033. https://doi.org/10.1016/j.jphotochem.2023.115033.

[2] Jiang H, Li Z, Kang Y, Ding L, Qiao S, Jia S, Luo W, Liu W. A two-photon fluorescent probe for Cu^{2+} based on dansyl moiety and its application in bioimaging. Sensor Actuator B Chem 2017;242:112–7. https://doi.org/10.1016/j.snb.2016.11.033.

[3] Pisagatti I, Crisafulli D, Pappalardo A, Trusso Sfrazzetto G, Notti A, Nastasi F, Parisi MF, Micali N, Gattuso G, Villari V. Photoinduced electron transfer in host-guest interactions of a viologen derivative with a didansyl-pillar[5]arene. Mater Today Chem 2022;24:100841. https://doi.org/10.1016/j.mtchem.2022.100841.

[4] Duarte F, Dobrikov G, Kurutos A, Santos HM, Fernández-Lodeiro J, Capelo-Martinez JL, Oliveira E, Lodeiro C. Enhancing water sensing via aggregation-induced emission (AIE) and solvatofluorochromic studies using two new dansyl derivatives containing a disulfide bound: pollutant metal ions detection and preparation of water-soluble fluorescent polymeric particles. Dyes Pigments 2023;218:111428. https://doi.org/10.1016/j.dyepig.2023.111428.

[5] Aliberti A, Vaiano P, Caporale A, Consales M, Ruvo M, Cusano A. Fluorescent chemosensors for Hg^{2+} detection in aqueous environment. Sensor Actuator B Chem 2017;247:727–35. https://doi.org/10.1016/j.snb.2017.03.026.

[6] Wei P, Xiao L, Gou Y, He F, Zhou D, Liu Y, Xu B, Wang P, Zhou Y. Fluorescent "on–off–on" probe based on copper peptide backbone for specific detection of Cu (II) and hydrogen sulfide and its applications in cell imaging, real water samples and test strips. Microchem J 2022;182:107848. https://doi.org/10.1016/j.microc.2022.107848.

[7] Srivastava P, Verma M, Sivakumar S, Patra AK. *Sens Actuators B Chem*, A smart FRET probe exhibiting a molecular keypad lock device based on rapid detection of nitric oxide mediated by Cu^{2+} ion, vol. 291; 2019. p. 478–84. https://doi.org/10.1016/j.snb.2019.04.093.

[8] Cai H, Liang Y, Huang L, Wang J. Relay detection of Cu^{2+} and bovine serum albumin by a dansyl derivative-based fluorescent probe. Spectrochim Acta Mol Biomol Spectrosc 2022;277:121281. https://doi.org/10.1016/j.saa.2022.121281.

[9] Wang Y, Zhou J, Zhao L, Xu B. A dual-responsive and highly sensitive fluorescent probe for Cu^{2+} and pH based on a dansyl derivative. Dyes Pigments 2020;180:108513. https://doi.org/10.1016/j.dyepig.2020.108513.

[10] Liu Y, Jiang B, Zhao L, Zhao L, Wang Q, Wang C, Xu B. A dansyl-based fluorescent probe for sensing Cu^{2+} in aqueous solution. Spectrochim Acta Mol Biomol Spectrosc 2021;261:120009. https://doi.org/10.1016/j.saa.2021.120009.

[11] Wang P, Zhou D, Chen B. High selective and sensitive detection of Zn(II) using tetrapeptide-based dansyl fluorescent chemosensor and its application in cell imaging. Spectrochim Acta Mol Biomol Spectrosc 2018;204:735–42. https://doi.org/10.1016/j.saa.2018.07.001.

[12] Wang P, Wu J. Highly selective and sensitive detection of Zn(II) and Cu(II) ions using a novel peptide fluorescent probe by two different mechanisms and its application in live cell imaging. Spectrochim Acta Mol Biomol Spectrosc 2019;208:140–9. https://doi.org/10.1016/j.saa.2018.09.054.

[13] Su P, Zhu Z, Wang J, Cheng B, Wu W, Iqbal K, Tang Y. A biomolecule-based fluorescence chemosensor for sequential detection of Ag^{+} and H_2S in 100% aqueous solution and living cells. Sensor Actuator B Chem 2018;273:93–100. https://doi.org/10.1016/j.snb.2018.06.037.

[14] Wang P, Zhou D, Chen B. A fluorescent dansyl-based peptide probe for highly selective and sensitive detect Cd^{2+} ions and its application in living cell imaging. Spectrochim Acta Mol Biomol Spectrosc 2019;207:276–83. https://doi.org/10.1016/j.saa.2018.09.029.

[15] Yu S, Gao L, Li R, Fu C, Meng W, Wang L, Li L. Ultrasensitive mercury ion and biothiol detection based on Dansyl-His-Pro-Gly-Asp-NH_2 fluorescent sensor. Spectrochim Acta Mol Biomol Spectrosc 2021;250:119246. https://doi.org/10.1016/j.saa.2020.119246.

[16] Li Y, Ren Z, Ge Y, Di C, Zhou J, Wu J, Jia L. A novel peptide fluorescent probe based on different fluorescence responses for detection of mercury species and hydrogen sulfide. Microchem J 2023;184:108160. https://doi.org/10.1016/j.microc.2022.108160.

[17] Pang X, Dong J, Gao L, Wang L, Yu S, Kong J, Li L. Dansyl-peptide dual-functional fluorescent chemosensor for Hg^{2+} and biothiols. Dyes Pigments 2020;173:107888. https://doi.org/10.1016/j.dyepig.2019.107888.

[18] Wang P, An Y, Wu J. Highly sensitive turn-on detection of mercury(II) in aqueous solutions and live cells with a chemosensor based on tyrosine. Spectrochim Acta Mol Biomol Spectrosc 2020;230:118004. https://doi.org/10.1016/j.saa.2019.118004.

[19] Li CL, hsuan Lu P, Lin SY, Wu AT. A turn-on dansyl-based fluorescent chemosensor for the recognition of Pb^{2+}. J Photochem Photobiol Chem 2019;385:112088. https://doi.org/10.1016/j.jphotochem.2019.112088.

[20] Tosato M, Asti M, Dalla Tiezza M, Orian L, Häussinger D, Vogel R, Köster U, Jensen M, Andrighetto A, Pastore P, Di Marco V. Highly stable silver(I) complexes with cyclen-based ligands bearing sulfide arms: a step toward silver-111 labeled radiopharmaceuticals. Inorg Chem 2020;59:10907–19. https://doi.org/10.1021/acs.inorgchem.0c01405.

[21] Wang ZF, Zhou XF, Wei QC, Qin QP, Li JX, Tan MX, Zhang SH. Novel bifluorescent Zn(II)–cryptolepine–cyclen complexes trigger apoptosis induced by nuclear and mitochondrial DNA damage in cisplatin-resistant lung tumor cells. Eur J Med Chem 2022;238:114418. https://doi.org/10.1016/j.ejmech.2022.114418.

[22] Blahut J, Bernášek K, Gálisová A, Herynek V, Císařová I, Kotek J, Lang J, Matějková S, Hermann P. Paramagnetic ^{19}F relaxation enhancement in nickel(II) complexes of N-trifluoroethyl cyclam derivatives and cell labeling for ^{19}F MRI. Inorg Chem 2017;56:13337–48.

[23] Cheung TL, Tam LKB, Tam WS, Zhang L, Kai HY, Thor W, Wu Y, Lam PL, Yeung YH, Xie C, Chau HF, Lo WS, Zhang T, Wong KL. Facile peptide macrocyclization and multifunctionalization via cyclen installation. Small Methods 2024:2400006. https://doi.org/10.1002/smtd.202400006.

[24] Surender EM, Comby S, Martyn S, Cavanagh B, Lee TC, Brougham DF, Gunnlaugsson T. Cyclen lanthanide-based micellar structures for application as luminescent [Eu(III)] and magnetic [Gd(III)] resonance imaging (MRI) contrast agents. Chem Commun 2016;52:10858–61. https://doi.org/10.1039/C6CC03092K.

[25] Naher M, Su C, Harmer JR, Williams CM, Bernhardt PV. Macrocyclic copper(II) complexes as catalysts for electrochemically mediated atom TransfeR. Inorg Chem 2024;63:6453–64. https://doi.org/10.1021/acs.inorgchem.4c00311.

[26] Annunziata A, Esposito R, Gatto G, Cucciolito ME, Tuzi A, Macchioni A, Ruffo F. Iron(III) complexes with cross-bridged cyclams: synthesis and use in alcohol and water oxidation catalysis. Eur J Inorg Chem 2018;2018:3304–11.

[27] Ollier C, Méndez-Ardoy A, Ortega-Caballero F, Jiménez-Blanco JL, Le Bris N, Tripier R. Extending the scope of the *C*-functionalization of cyclam via copper(I)-Catalyzed alkyne–azide cycloaddition to bifunctional chelators of interest. J Org Chem 2024;89:5988–99. https://doi.org/10.1021/acs.joc.3c02854.

[28] Yu Y, Tan P, Huang X, Tao J, Liu Y, Zeng RJ, Chen M, Zhou S. Homogeneous activation of peroxymonosulfate using a low-dosage cross bridged cyclam manganese(II) complex for organic pollutant degradation via a nonradical pathway. J Hazard Mater 2020;394:122560. https://doi.org/10.1016/j.jhazmat.2020.122560.

[29] Wong JKH, Todd MH, Rutledge PJ. Recent advances in macrocyclic fluorescent probes for ion sensing. Molecules 2017;22:200. https://doi.org/10.3390/molecules22020200.

[30] Ozay H, Gungor Z, Yilmaz B, Ilgin P, Ozay O. Dual use of colorimetric sensor and selective copper removal from aqueous media with novel p(HEMA-co-TACYC) hydrogels: cyclen derivative as both monomer and crosslinker. J Hazard Mater 2020;389:121848. https://doi.org/10.1016/j.jhazmat.2019.121848.

[31] Fang X, Wang S, Wang Q, Gong J, Li L, Lu H, Xue P, Ren Z, Wang X. A highly selective and sensitive fluorescence probe based on BODIPY-cyclen for hydrogen sulfide detection in living cells and serum. Talanta 2024;268:125339. https://doi.org/10.1016/j.talanta.2023.125339.

[32] Tomczyk MD, Matczak K, Skonieczna M, Chulkin P, Denel-Bobrowska M, Różycka D, Rykowski S, Olejniczak AB, Walczak K. Synthesis and in vitro cytotoxic activity of dye-linker-macrocycle conjugates with variable linker length and components. Bioorg Chem 2023;140:106782. https://doi.org/10.1016/j.bioorg.2023.106782.

[33] Aoki S, Kawatani H, Goto T, Kimura E, Shiro M. A double-functionalized cyclen with carbamoyl and dansyl groups (cyclen = 1,4,7,10-tetraazacyclododecane): a selective fluorescent probe for Y^{3+} and La^{3+}. J Am Chem Soc 2001;123:1123–32. https://doi.org/10.1021/ja0033786.

[34] Lowe MP, Parker D. pH Switched sensitisation of europium(III) by a dansyl group. Inorg Chim Acta 2001;317:163–73. https://doi.org/10.1016/S0020-1693(01)00346-2.

[35] Siters KE, Fountain MA, Morrow JR. Selective binding of Zn^{2+} complexes to human telomeric G-quadruplex DNA. Inorg Chem 2014;53:11540–51. https://doi.org/10.1021/ic501484p.

[36] Del Mundo IMA, Siters KE, Fountain MA, Morrow JR. Structural basis for bifunctional zinc(II) macrocyclic complex recognition of thymine bulges in DNA. Inorg Chem 2012;51:5444–57. https://doi.org/10.1021/ic3004245.

[37] Kim JY, Sarkar S, Bobba KN, Huynh PT, Bhise A, Yoo J. Development of dansyl based copper(ii) complex to detect hydrogen sulfide in hypoxia. Org Biomol Chem 2019;17:7088–94. https://doi.org/10.1039/C9OB00948E.

[38] O'neil LL, Wiest O, Selective A. Noncovalent assay for base flipping in DNA. J Am Chem Soc 2005;127:16800–1. https://doi.org/10.1021/ja056274+.

[39] Rivas C, Stasiuk GJ, Sae-Heng M, Long NJ. Towards understanding the design of dual-modal MR/fluorescent probes to sense zinc ions. Dalton Trans 2015;44:4976–85. https://doi.org/10.1039/C4DT02981J.

[40] Yang L, Zhao J, Wang J, Han G, Liu B, Zhang W, Fu Y, Han MY, Wang Z, Zhang Z. An azacyclo-localizing fluorescent probe for the specific labeling of lysosome and autolysosome. Talanta 2020;216:120941. https://doi.org/10.1016/j.talanta.2020.120941.

[41] Xue G, Bradshaw JS, Song H, Bronson RT, Savage PB, Krakowiak KE, Izatt RM, Prodi L, Montalti M, Zaccheroni N. A convenient synthesis and preliminary photophysical study of novel fluoroionophores: macrocyclic polyamines containing two dansylamidoethyl side arms. Tetrahedron 2001;57:87–91. https://doi.org/10.1016/S0040-4020(00)00999-6.

[42] Fabbrizzi L, Foti F, Licchelli M, Maccarini PM, Sacchi D, Zema M. Light-emitting molecular machines: pH-induced intramolecular motions in a fluorescent nickel(II) scorpionate complex. Chem Eur J 2002;8:4965–72. https://doi.org/10.1002/1521-3765(20021104)8:21<4965::AID-CHEM4965>3.0.CO;2-X.

[43] Bergamini G, Sottilotta A, Maestri M, Ceroni P, Vögtle F. Cyclam-cored dendrimers appended with four dendrons of two different types: intradendrimer energy transfer. Chem Asian J 2010;5:1884–95. https://doi.org/10.1002/asia.201000170.

[44] Pillai ZS, Ceroni P, Kubeil M, Heldt JM, Stephan H, Bergamini G. Dendrimers as Nd^{3+} ligands: effect of generation on the efficiency of the sensitized lanthanide emission. Chem Asian J 2013;8:771–7. https://doi.org/10.1002/asia.201201065.

[45] Branchi B, Ceroni P, Bergamini G, Balzani V, Maestri M, Van Heyst J, Lee SK, Luppertz F, Vögtle F. A cyclam core dendrimer containing dansyl and oligoethylene glycol chains in the branches: protonation and metal coordination. Chem Eur J 2016;12:8926–34. https://doi.org/10.1002/chem.200601129.

[46] Montalti M, Credi A, Prodi Mg L, Montalti M, Credi A, Prodi LGM. Handbook of photochemistry. third ed. Boca Raton: Taylor & Francis; 2006. BOCA.

[47] Macdougall D, Crummett WB. Guidelines for data acquisition and data quality evaluation in environmental chemistry. Anal Chem 1980;52:2242–9. https://doi.org/10.1021/ac50064a004.

[48] Long GL, Winefordner JD. Limit of detection A closer look at the iupac definition. Anal Chem 1983;55:713A–24A. https://doi.org/10.1021/ac00258a724.

[49] Mocanu S, Ionita G, Matei I. Solvatochromic characteristics of dansyl molecular probes bearing alkyl diamine chains. Spectrochim Acta Part A Mol Biomol Spectrosc 2020;237:118413. https://doi.org/10.1016/j.saa.2020.118413.

[50] Oliveira E, Baptista RMF, Costa SPG, Raposo MMM, Lodeiro C. Solvatochromic Effects of bis(indolyl)thienylaril derivatives as new Colored Materials. Photochem Photobiol Sci 2014;13:492–8. https://doi.org/10.1039/C3PP50352F.

[51] Alam P, Leung NLC, Zhang J, Kwok RTK, Lam JWY, Tang BZ. AIE-based luminescence probes for metal ion detection. Coord Chem Rev 2021;429:213693. https://doi.org/10.1016/j.ccr.2020.213693.

[52] Wang H, Zhao E, Lam JWY, Tang BZ. AIE luminogens: emission brightened by aggregation. Mater Today 2015;18:365–77. https://doi.org/10.1016/j.mattod.2015.03.004.
[53] Koucký F, Kotek J, Císařová I, Havlíčková J, Kubíček V, Hermann P. Transition metal complexes of cyclam with two 2,2,2-trifluoroethylphosphinate pendant arms as probes for ^{19}F magnetic resonance imaging. Dalton Trans 2023;52:12208–23. https://doi.org/10.1039/D3DT01420G.
[54] Le Roy MM, Héry S, Saffon-Merceron N, Platas-Iglesias C, Troadec T, Tripier R. A phosphine oxide-functionalized cyclam as a specific, copper(II) chelator. Inorg Chem 2023;62:8112–22. https://doi.org/10.1021/acs.inorgchem.3c00329.
[55] Naher M, Su C, Harmer JR, Williams CM, Bernhardt PV. Macrocyclic copper(II) complexes as catalysts for electrochemically mediated atom transfer. Inorg Chem 2024;63:6453–64. https://doi.org/10.1021/acs.inorgchem.4c00311.
[56] Li X, Pan L, Yang F, Yang L. Blue carbon dot-based portable smartphone platform for visualization of copper(II). ACS Appl Nano Mater 2022;5:9252–9. https://doi.org/10.1021/acsanm.2c01595.
[57] Lelong E, Suh JM, Kim G, Esteban-Gómez D, Cordier M, Lim MH, Delgado R, Royal G, Platas-Iglesias C, Bernard H, Tripier R. Inorg Chem 2021;60:10857–72.
[58] Brown AM, Butman JL, Lengacher R, Vargo NP, Martin KE, Koller A, Śmiłowicz D, Boros E, Robinson JR. *N,N*-Alkylation clarifies the role of *N*- and *O*-protonated intermediates in cyclen-based ^{64}Cu radiopharmaceuticals. Inorg Chem 2023;62:1362–76. https://doi.org/10.1021/acs.inorgchem.2c02907.
[59] Almada S, Maia LB, Waerenborgh JC, Vieira BJC, Mira NP, Silva ER, Cerqueira F, Pinto E, Alves LG. Cyclam-based iron(III) and copper(II) complexes: synthesis, characterization and application as antifungal agents. New J of Chem 2022;46:16764–70. https://doi.org/10.1039/D2NJ03161B.
[60] Zhang H, Song J, Wang S, Song Q, Guo H, Li Z. Recent progress in macrocyclic chemosensors for lead, cadmium and mercury heavy metal ions. Dyes Pigments 2023;216:111380. https://doi.org/10.1016/j.dyepig.2023.111380.
[61] Tosato M, Randhawa P, Asti M, Hemmingsen LBS, O'Shea CA, Thaveenrasingam P, Sauer SPA, Chen S, Graiff C, Menegazzo I, Baron M, Radchenko V, Ramogida CF, Di Marco V. Capturing mercury-197m/g for auger electron therapy and cancer theranostic with sulfur-containing cyclen-based macrocycles. Inorg Chem 2024;63:14241–55. https://doi.org/10.1021/acs.inorgchem.4c02418.
[62] Gans P, Sabatini A, Vacca A. Investigation of equilibria in solution. Determination of equilibrium constants with the HYPERQUAD suite of programs. Talanta 1996;43:1739–53. https://doi.org/10.1016/0039-9140(96)01958-3.